JPhys Energy



**PAPER** • **OPEN ACCESS**

# Radiation versus environmental degradation in unencapsulated metal halide perovskite solar cells

To cite this article: Megh N Khanal *et al* 2024 *J. Phys. Energy* **6** 045001

Journal of Physics: Energy

PAPER

# Radiation versus environmental degradation in unencapsulated metal halide perovskite solar cells

Megh N Khanal[1,6], Vincent R Whiteside[1], Mritunjaya Parashar[2], Tamara Merckx[3,4,5], Mohin Sharma[2], Yinghuan Kuang[3,4,5], Aranzazu Aguirre[3,4,5], Hadi Afshari[1], Sarallah Hamtaei[3,4,5], Tom Aernouts[3,4,5], Bart Vermang[3,4,5], Bibhudutta Rout[2] and Ian R Sellers[1,6,*]

[1] Department of Physics and Astronomy, Nielsen Hall, University of Oklahoma, Norman, OK 73019, United States of America
[2] Department of Physics, University of North Texas, Denton, TX 76203, United States of America
[3] Imec, imo-imomec, Thin Film PV Tech.—partner in Solliance, Thor Park 8320, 3600 Genk, Belgium
[4] EnergyVille, imo-imomec, Thor Park 8320, 3600 Genk, Belgium
[5] Hasselt University, imo-imomec, Martelarenlaan 42, 3500 Hasselt, Belgium
[6] Department of Electrical Engineering, 230 Davis Hall, University at Buffalo, Buffalo, NY 14260, United States of America
* Author to whom any correspondence should be addressed.

**E-mail:** isellers@buffalo.edu

**Keywords:** metal halide perovskites, space photovoltaics, radiation tolerance

Supplementary material for this article is available online

OPEN ACCESS

RECEIVED
22 January 2024

REVISED
25 June 2024

ACCEPTED FOR PUBLICATION
19 July 2024

PUBLISHED
12 August 2024



## Abstract

Here, the radiation hardness of metal halide perovskite solar cells exposed to space conditions versus the effects of environmental degradation are assessed. The relative response of the constituent layers of the architecture to radiation is analyzed, revealing a general resilience of the structure when assessed across varying proton energy levels and fluences. However, despite the tolerance of the structure to irradiation, sensitivity to environmental degradation is observed during the transit of the device between the radiation and characterization facilities. Experimental evidence suggests the $NiO_x$/perovskite interface is particularly sensitive to the effects of humidity and/or temperature exposure, while the irradiation of the devices appears to induce thermally activated annealing: improving the solar cells upon radiation exposure.

## 1. Introduction

Perovskite devices have seen a remarkable increase in performance in recent years [1–3]. While stability has proven challenging, optimization and development of diverse material combinations have resulted in more robust performance, particularly at high temperatures and in practical environmental conditions [4, 5]. In particular, the double cation (FA, Cs)Pb(I, Br)$_3$ solar cell has been gaining popularity for space-based applications due to its remarkable stability [2, 6], resistivity against radiation [3, 7, 8], and is emerging as a candidate for the upper layer for perovskite-silicon tandem solar cells [9, 10]. The high demand for space-based solar cells is pushing research and innovation into an accelerated phase. The environment in space has always been challenging for successful space missions. This is due to radiation from protons, electrons, and other heavier ions [8, 9]; as well as, high vacuum conditions, space debris, and thermal cycling in various orbits and mission conditions [10].

Amongst these challenging conditions, degradation induced from radiation has been extensively studied and has been considered along with the large temperature variations as the most prominent degradation process when evaluating perovskites for space. This is primarily due to the extreme damage radiation exposure causes in many PV materials [11, 12]. When considering potential applications, most satellites are in Low Earth Orbit (LEO), which is typically dominated by low energy protons and electrons [13, 14], the fluence of which is exacerbated when considering more demanding orbits such as the polar or High Earth Orbits (HEO) that are of interest for next generation satellite constellations, as well as for GPS and internet applications [13].

Despite their relatively soft nature, several groups from around the world have now demonstrated the tolerance of perovskites to radiation and as such some of the focus has shifted towards identifying effective (stable and tolerant) transport layers [15, 16]. Under practical space conditions these transport layers must possess attributes such as: efficient charge extraction, resilience to radiation induced effects, thermal stability, and reliable performance. Titanium dioxide ($TiO_2$), tin dioxide ($SnO_2$), and lithium fluoride (LiF) have gained popularity as electron transport layers (ETLs) [17, 18], while organic materials like Spiro-OMeTAD and poly[bis(4-phenyl)(2,4,6-trimethylphenyl)amine] (PTAA) are popular as hole transport layers (HTLs). However, recently it has been considered that a possible cause of instability or a weakness of perovskite devices in extreme conditions is with the selection of the HTL due to poor chemical stability and low hole mobility when using Spiro and PTAA [19, 20]. Various inorganic and/or organic compounds have been studied as potential candidates for HTL [19, 20]. The exploration and enhancement of HTLs offers more opportunities for further scientific improvement.

Previous experiments [21, 22] have investigated the effects of proton irradiation on various solar cells including the space dominant III–V's such as GaAs [23, 24] as well as, other potential systems like silicon (used on the international space station) and CIGS [25, 26]. At present, several works have focused on a wide range of perovskite materials, transport layers, and device architectures to gauge their effectiveness under extreme space environment [3, 6, 17, 18]. Metal halide perovskite absorbers have exhibited remarkable resistance to radiation-induced damage [12, 27, 28–32] as well as an extreme thermal environment [6], often displaying a self-healing property [28, 33].

While replicating the exact space conditions in a ground-based lab is challenging, these experiments provide valuable insights into fundamental considerations while assessing device performance and understanding device behavior in the space environment [3, 14, 31]. Moreover, little is known of the degradation of the packaged solar cells pre-launch when the devices are likely exposed to high humidity and temperature for several months. At this stage of research, it is crucial to comprehend the impact of radiation damage on each layer within these solar cells and to develop strategies to mitigate these effects. Such studies play a crucial role in furthering perovskite research for space applications. Here, the radiation tolerance of metal halide perovskite solar cells was studied under conditions replicating space operations, as well as relative to devices exposed to terrestrial pre-launch conditions (this is mimicked by a lack of encapsulation during transit under high temperature and humidity). The lack of encapsulation is postulated to represent accelerated potential pre-launch degradation processes at US facilities in Florida or Texas.

Additionally, the effects of irradiation and environmental conditions on the $NiO_x$ HTL were systematically assessed. The structure of the devices investigated consisted of a blade-coated $Cs_{0.2}FA_{0.8}Pb(I_{0.947}Br_{0.053})_3$ perovskite (1.6 eV, ∼500 nm) absorber (to our knowledge the first time such a system has been evaluated for space) layer deposited between a $NiO_x$ HTL (15 nm) by magnetron sputtering and a combination of LiF (0.8 nm), C60 (60 nm), and BCP (5 nm) all by thermal evaporation, respectively, as the ETL. This structure was encapsulated between ITO layers on both surfaces, and with gold grids (100 nm in thickness on ITO) by thermal evaporation were then used as metal contacts. Experimental details of cell fabrication are in supplementary information (SI-1).

## 2. Results and discussion

Assessing the energy distribution and flux of radiation exposure in devices is fundamental to assessing their effects on material stability in space. To enable a more comprehensive analysis of the degradation of the device, the proton penetration depth and vacancy generation were studied using the Stopping and Range of Ions in Matter (SRIM) simulation as shown in figure 1. SRIM employs a Monte Carlo Simulation for simulating the interaction of energetic ions with their energy loss and trajectory in matter. As such, SRIM provides valuable insights into interaction processes and the relative contribution of ionizing (IEL) and non-ionizing energy (NIEL) loss in the system under investigation. Prior to the experiments, SRIM simulations are performed [34] to calculate the required proton energy for interaction with the various layers and interfaces within the device structure, enabling proper assessment of the stability of the architecture as a whole [12, 35]. Detailed information pertaining to this analysis can be found in figure 1. As shown in figures 1(a) and (c), 45 keV protons penetrate the perovskite layer of the device, instigating energy loss and degradation directly in the absorber layer.

Notably, when considering the elemental vacancies analysis shown in figure 1(c), under 45 keV irradiation, the primary atomic displacement within the perovskite layer is the generation of hydrogen vacancies, followed by iodine and lead. This reflects the composition of the device and the defect generation (vacancies and/or interstitials) observed previously in these systems [3, 12] which under the low energy irradiation here predominately affect the ETL and perovskite absorber in the structure. The impact of proton

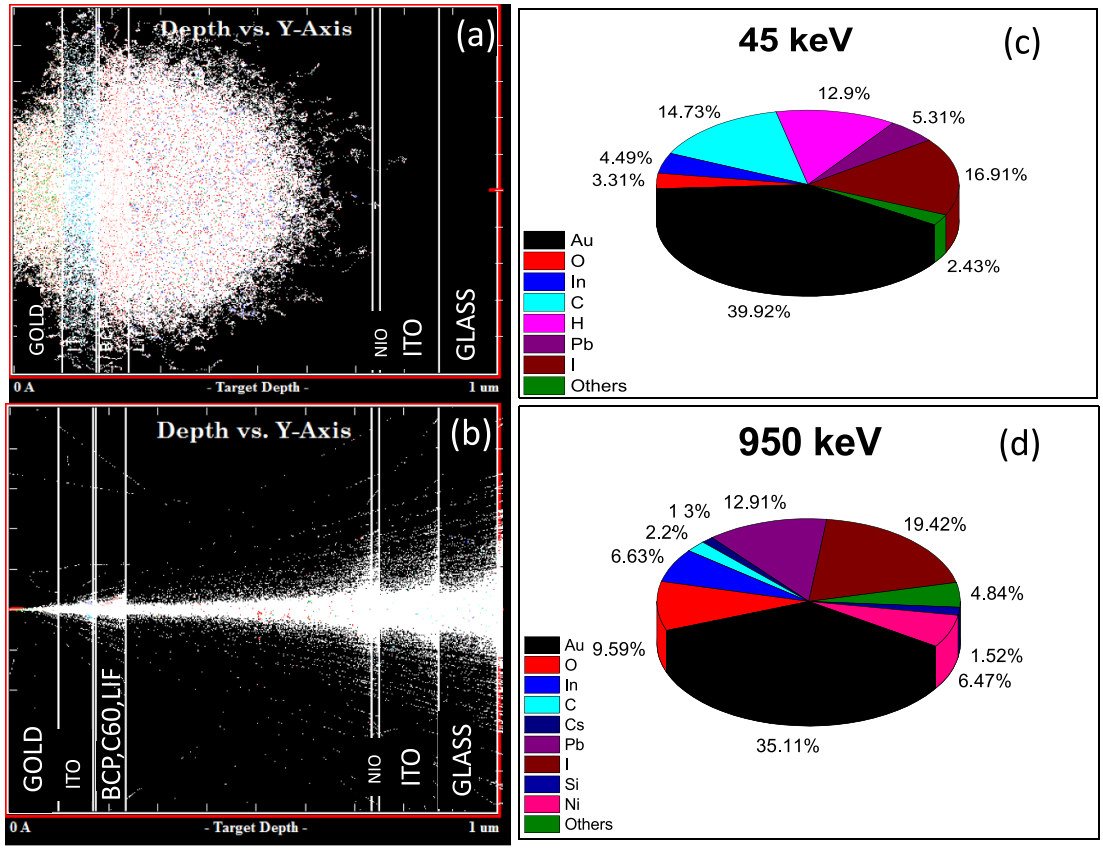


**Figure 1.** Range of ions and associated damage profile in the metal halide perovskite device under investigation when irradiated with: (a) 45 keV and (b) 950 keV protons. The vacancies and their elemental compositions generated due to these exposures simulated from SRIM are shown for the case of 45 keV and 950 keV exposure in (c) and (d), respectively.

irradiation on the $NiO_x$ HTL is small, reflecting the limited proton penetration into this layer at 45 keV (see figure 1(a)).

To mimic deeper penetration of protons within the device structure, SRIM simulations were conducted to assess vacancy generation resulting from a much higher irradiation energy of 950 keV. These simulations are shown in figures 1(b) and (d). For these higher energy protons SRIM indicates most of the damage will be at the front of the cell (HTL side), leading to the generation of vacancies in the indium tin oxide layer and the glass substrate. The high energy protons also produce significant exposure of the $NiO_x$ HTL to radiation damage resulting in substantial increments in vacancies (figure 1(d)) for both nickel and oxygen, as compared to 45 keV shown in figure 1(c).

In this experiment, two proton energies (45 keV and 950 keV) each with low and high fluence ($10^{11}$ and $10^{13}$ protons $cm^{-2}$, respectively) were used to irradiate the devices. Since the side typically illuminated—the glass substrate—is very thick, proton irradiation was conducted through the upper electrode (Au) surface. This enabled variations in irradiation energy and controlled exposure of designated regions of the solar cells, without significant energy loss that would occur if exposure was through the glass substrate. The proton trajectory is shown in figures 1(a) and (b) for the low (45 keV) and high (950 keV) radiation, respectively.

The 45 keV protons traverse the ETL and terminate in the perovskite absorber creating significant loss due to NIEL. This is reflected in the high vacancy (or defect) generation as demonstrated from SRIM calculations in figure 1(c). In the case of the 950 keV proton beam, the proton traverses the entire solar cell structure terminating in the glass substrate as seen in figure 1(b). As such, these high-energy protons have very limited interaction within the device stack, primarily resulting in IEL with significantly fewer vacancies generated compared to low-energy protons. This is evident in figure 1(d), which shows the vacancy generation estimated by SRIM for the high-energy protons.

To understand the relative contribution of IEL and NIEL, or to induce additional defects that mimic longer durations in space, the solar cells were exposed (at 45 keV and 950 keV) to fluences of $10^{11}$ protons $cm^{-2}$ and $10^{13}$ protons $cm^{-2}$. In total, 35 devices were studied to gather statistics, with seven different devices irradiated at each condition (45 keV − $10^{11}$; 45 keV − $10^{13}$; 950 keV − $10^{11}$; and

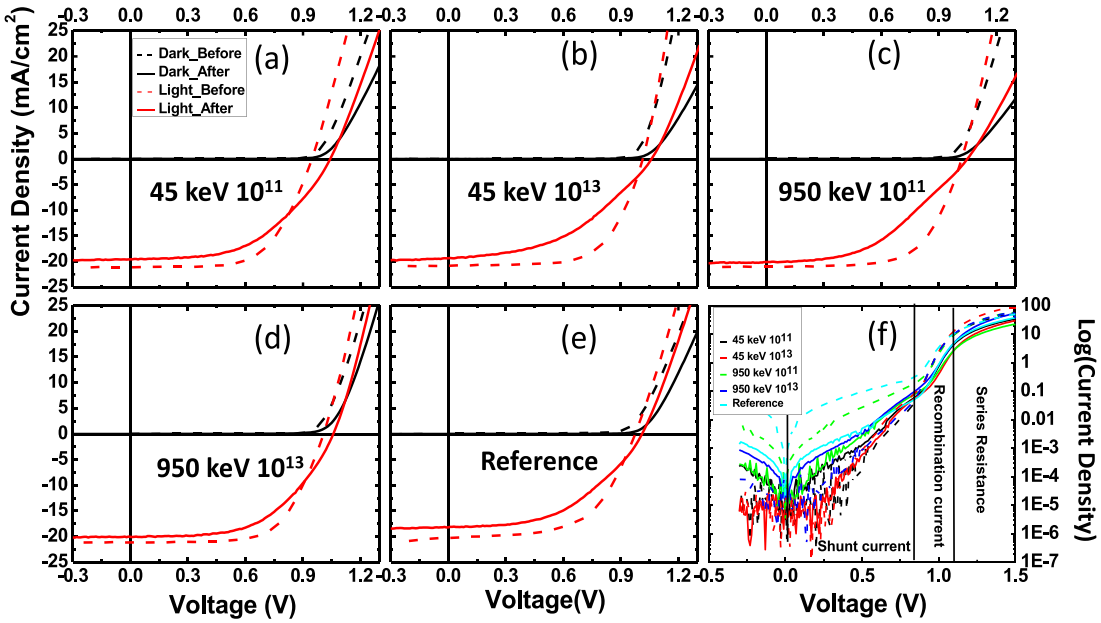


**Figure 2.** Current density–voltage ($J$–$V$) characteristics under different irradiation conditions are shown before (dashed) and after (solid) irradiation in (a) and (b) for 45 keV protons, and in (c) and (d) for 950 keV protons. The $J$–$V$ response for a representative reference traveler device is shown in (e), and a comparison of dark $J$–$V$ of all the devices before and after transit to the ion beam facility are shown in (f).

950 keV − $10^{13}$ protons cm$^{-2}$). The remaining 7 devices were used as travelers (references) that were not irradiated but traveled between the University of Oklahoma (OU) and the University of North Texas (UNT) ion beam facility [36] to assess any environmental effects or perturbations experienced by the devices in transit. These travelers *did not* undergo proton irradiation. Since the goal was to understand the device response and effectiveness under a more *practical* environment, the devices were transported with containers sealed with nitrogen, but not vacuum-sealed.

The current density–voltage ($J$–$V$) and external quantum efficiency (EQE) responses of devices were tested before and after irradiation to understand device degradation due to radiation exposure *and/or* traveling. For $J$–$V$ measurement, a Newport solar simulator with AM 1.5 G filter was used. A Keithley 2400 voltage and current source at a sweep rate of 333 mV s$^{-1}$, and a dwell time of 30 ms was used to apply the bias voltage and measure the resulting dark and light induced current. Prior to measurement, the devices were light soaked at 1-sun AM 1.5 G equivalent for 25 min before the $J$–$V$ characteristics were taken [37]. EQE measurements were conducted using a current preamplifier and a Stanford Research Systems lock-in amplifier. A Xenon lamp was used as light source, and the reference spectrum was collected via a calibrated silicon photodiode.

Figure 2 shows the room temperature $J$–$V$ before (dashed) and after (solid) proton irradiation for various energy and fluences. Figures 2(a) and (b) show the before and after $J$–$V$ when exposed to 45 keV at fluences of $1 \times 10^{11}$ protons cm$^{-2}$ and $1 \times 10^{13}$ protons cm$^{-2}$, respectively. Figures 2(c) and (d) show the effects of a higher proton irradiation energy of 950 keV, again for fluences of $1 \times 10^{11}$ protons cm$^{-2}$ and $1 \times 10^{13}$ protons cm$^{-2}$, respectively. Figure 2(e) shows the $J$–$V$ response of a representative reference traveler device, while figure 2(f) shows the dark $J$–$V$ for all devices before and after transit to the ion beam facility with or without irradiation. The dashed lines represent prior to irradiation and/or transit, while solid lines are those measured after the device returned to OU. When analyzing the curves under illumination (red lines), a small increase in open circuit voltage ($V_{oc}$) is apparent after irradiation. This appears to be a result of parasitic transport in the devices since the short circuit current density ($J_{sc}$) also experienced a decrease with a significant increase in series resistance, which manifests itself in a noticeable reduction in fill factor (*FF*).

Interestingly, these properties are observed in all the devices assessed at all radiation conditions, including the reference devices. This restriction of carrier-extraction reflected in the loss of $J_{sc}$ and *FF*—implies inhibited transport in the device, likely at one, or both, of the interfaces between the transport layers and the perovskite absorber. Again, the *FF* decreases significantly for both the 'travelers' and irradiated devices, suggesting this degradation is not predominately due to irradiation of the devices. When considering the dark $J$–$V$s measured before (dashed) and after (solid) transit and/or irradiation, compared in figure 2(f),

an apparent decrease in dark current is observed after the devices experienced external perturbations and returned to Oklahoma. This surprising result manifests itself in the increase in $V_{oc}$ observed upon irradiation for the 'after' devices seen in figures 2 (solid responses).

While a reduction in dark current and the consequential increase in $V_{oc}$ typically result in improved performance, as these are typically linked to non-radiative processes—here, the performance of the solar cell decreases despite apparent improvements in dark *J–V*. Such behavior has been observed previously in perovskite solar cells in which parasitic barriers inhibit carrier extraction, particularly at low temperatures [38, 39], and in III–V quantum dot solar cells where trapped carriers distort the dark current due to carrier localization [40]. As discussed further below, in the devices under investigation here, limited carrier extraction at a parasitic barrier and/or reduced extraction via the charge transporting layers [41] is the likely cause of the decreased dark current levels and increase in $V_{oc}$ after exposure.

The limited extraction of carriers after transit and/or irradiation is supported by a decrease in $J_{sc}$, *FF,* and power conversion efficiency (*PCE)* after irradiation (solid red < dashed red) in figure 2. While degradation upon irradiation might be expected, the lack of a qualitative trend in the loss of performance for the various irradiation conditions shown in figure 2(a) through (d), and similar effects in lost performance for the references imply that radiation exposure is not the dominant loss mechanism in the devices under investigation. Moreover, several recent studies have also indicated that perovskite materials and devices display remarkable tolerance to radiation exposure [3, 7, 8, 12, 28, 31]. As such, here it appears that the dominant loss process is related to environmental factors experienced during transit between Oklahoma and Texas for radiation exposure in the humid conditions of the Plains region. This mirrors the environmental conditions these systems might encounter prior to space launch in Florida or Texas.

To assess this hypothesis further, and to gain a more statistical understanding of device performance and degradation, the photovoltaic parameters ($J_{sc}$, $V_{oc}$, *FF, and PCE*) of several devices for each irradiation condition were analyzed. As is clear from the reference (or traveler) *J–V* in Figure 2(e), all the solar cell parameters were affected by transit. To obtain a more qualitative analysis of the effects due to irradiation *only*, any effects experienced (after/before) by the traveler devices were used as a reference (background), and subsequently removed from the samples exposed to proton irradiation; assuming all devices experience the same environmental degradation during to transit between facilities. Dividing the factor of change in the irradiated devices with the change in the reference cells gives a qualitative assessment of the effects of radiation *only* on the devices. A remaining factor of >1 suggests improvement in device performance, while remaining factor of <1 indicates degradation in device quality after irradiation. As such, figure 3 displays the PV parameters before and after irradiation *only*, to gauge the effects of radiation *independently* on those devices that were exposed. The parameter plots before removing any environmental effects can be found in the supplementary information figure (SI-2).

Figure 3(a) shows the remaining factor of the extracted $J_{sc}$ of all irradiated devices, indicating an increase in $J_{sc}$ after irradiation. Despite the apparent increase in $V_{oc}$ as shown in figure 2; the adjusted values presented in figure 3(b) show minimal changes in $V_{oc}$ (within errors) due to irradiation *after* factoring out the environmental effects. Figures 3(c) and (d) also indicate neither *FF* nor *PCE* have been significantly affected by irradiation. These adjusted PV parameters are consistent with previous findings [12, 28, 32] that show perovskite solar cells are relatively radiation tolerant, and that here, the devices assessed are more affected by environmental conditions experienced during transit than by irradiation. While radiation tolerance is important, to deploy these cells in practical conditions requires device robustness against heat and humidity (launch conditions) as well as the space-like environment [42]. Therefore, this study is pertinent in assessment of the potential issues with terrestrial transportation and storage of perovskite solar cells prior to launch if proper encapsulation and/or layer design is not carefully considered.

Notably, while there are relatively large dispersions, the improvement in $J_{sc}$, $V_{oc}$, *FF*, and *PCE* after 45 keV at $10^{11}$ protons $cm^{-2}$ and 950 keV at $10^{13}$ protons $cm^{-2}$ is greater than the change in the other two irradiating conditions (45 keV at $10^{13}$ protons $cm^{-2}$ and 950 keV at $10^{11}$ protons $cm^{-2}$). The relative changes deduced across the various devices reflect to some extent the relative change in EQE with respect to the AM1.5 G solar spectrum such that significant changes at wavelengths <∼550 nm experience higher relative solar irradiance and therefore greater $J_{sc}$, as compared with respect to changes in the devices at longer wavelengths (>550 nm) with less solar resource. While care must be taken when making any quantitative conclusions, it is possible that under the conditions of lower energy/low fluence (45 keV at $10^{11}$ protons $cm^{-2}$) and high energy/high fluence (950 keV at $10^{13}$ protons $cm^{-2}$) that appear to improve the remaining factor in figures 3, even 'healing' the devices, that the contribution of IEL to NIEL is important. This has been shown to be the case for perovskites in several recent studies in which the amount of heat generated in the perovskite absorber and transport layers via IEL, as opposed to the NIEL upon radiation

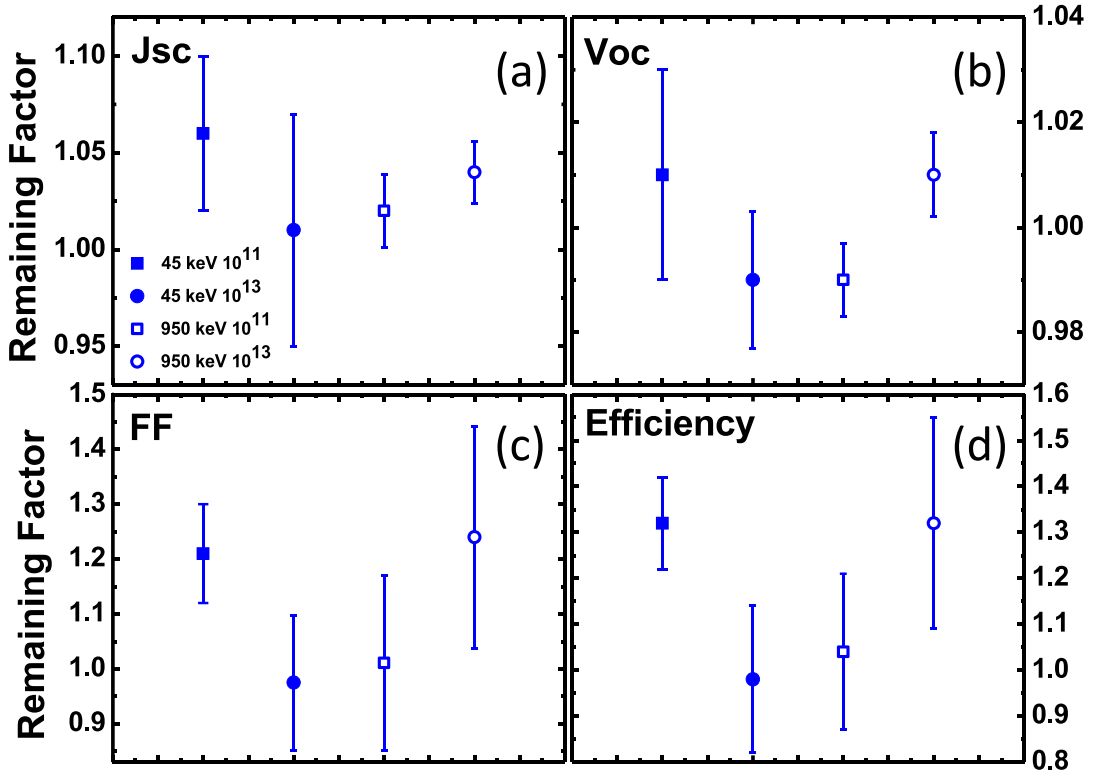


**Figure 3.** Remaining factor of the extracted *J–V* parameters: (a) $J_{sc}$, (b) $V_{oc}$, (c) *FF*, and (d) *PCE*, before and after irradiation as determined after removing environmental effects experienced by the traveler reference devices. The error bars reflect the dispersion/distribution in this value reflected by 35 individual devices. The open and solid symbols represent devices exposed to 950 keV and 45 keV protons, respectively, while the square symbols reflect a fluence of $\sim 10^{11}$ protons cm$^{-2}$ and the circular symbols show the device exposed to fluences of $10^{13}$ protons cm$^{-2}$.

exposure, plays a crucial beneficial role in perovskite devices due to local annealing. This phenomenon appears to improve transport and interfacial quality in these systems [28, 29, 33, 43].

To understand the effects of irradiation and environment conditions on specific layers throughout the device, EQE was also performed before and after irradiation. Figure 4(a) shows EQE of the reference device (black) and a device after irradiation (red) (45 keV at $10^{11}$ protons cm$^{-2}$) to provide a qualitative picture of the comparison of these devices. Prior to irradiation, the absorption was approximately 85% at shorter wavelengths ($<\sim$550 nm), declining to around 60% at wavelengths beyond $\sim$550 nm, as seen in figures 4(a) and (b). Additional EQE data for all conditions can be found in supporting information (S2).

In figure 4, when comparing the EQE of both the irradiated and traveler (reference) devices before and after transit, a clear reduction of the EQE is evident across the entire EQE spectrum as shown in figures 4(a) and (b). The difference in EQE before and after transit and/or irradiation are shown in blue and magenta for the irradiated and reference cells in figures 4(a) and (b), respectively. The reduction (or change) in EQE is observed to be slightly higher at shorter wavelengths, which represents the front side of the cell—at the HTL layer—where light enters the structure (see figure 4(c)), than at the back of the cell (ETL layer). The orientation of illumination is shown schematically in figure 4(c).

Notably, in figures 4(a) and (b), there is little or no change in the band gap of the perovskite absorber with either the irradiated or reference devices when comparing before and after ($\sim$800 nm) spectra. These data imply the degradation in device performance is dominated by losses at the perovskite/$NiO_x$ interface region. Figure 4(d) shows the change in EQE before and after irradiation for all cases as well as, for the traveler. The shaded regions reflect the regions of the device in which short (grey, 300–420 nm), mid (orange, 420–740 nm), and long (gold, >740 nm) wavelengths of light are absorbed in the device structure as illustrated schematically above, in figure 4(c). These regions reflect the HTL, absorber, and ETL layers, respectively. The negative values observed in all cases indicate reduction in absolute EQE after transit to UNT for all samples; *irradiated or not*. The differential EQE reduces sharply in light gray region (HTL side of device) for all irradiating cases as well as the reference device (black). This suggests HTL was affected more significantly by the environmental conditions during transit, rather than due to irradiation induced degradation. This hypothesis is further supported by inspection of the relative EQE of the proton irradiation

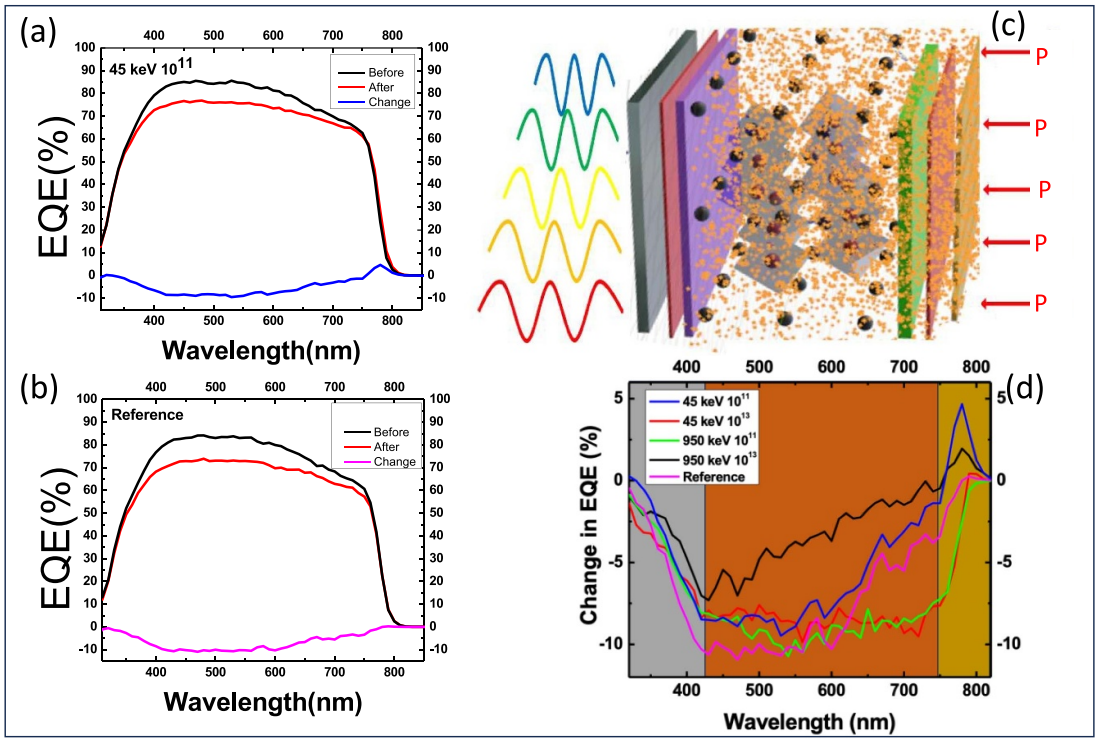


**Figure 4.** Comparison of the EQE before (black solid line) and after (red solid line) irradiation by; (a) 45 keV at $10^{11}$ protons $cm^{-2}$, and (b) for the reference traveler device. The change (or difference) in response before and after transit and/or irradiation is shown in blue and magenta for the irradiated and reference devices sown in (a) and (b), respectively. (c) Cartoon representation of the device structure and orientation of the light illumination and relative proton irradiation direction with respect to the device, and (d) a comparison of the relative change in EQE, shown for all devices irradiated in this study.

solar cells before and after dark-ambient storage for 3 weeks shown in the supplementary information (SI-4). These data show an improvement in the EQE of the perovskite absorber after well known dark-self-healing at ambient conditions. [12, 28, 44] However, no improvements at the HTL region of the devices are evident in these data indicating permanent losses at the $NiO_x$/MHP interface.

Careful consideration of the orange shaded region in figure 4(d) further supports the hypothesis that the EQE has been more affected by extrinsic losses due to traveling than radiation exposure since, the irradiated devices that also traveled have less significant losses (or change) in EQE as compared to the nonirradiated traveler cells; which on inspection actually suggests improvement of device quality after irradiation. This supports previous findings of improvements in perovskite solar cell performance after high energy radiation [3, 12, 28, 33]. This is evident in figure 4(d) when comparing the change in EQE for exposure to 45 keV at $10^{11}$ protons $cm^{-2}$ (blue) and 950 keV at $10^{13}$ protons $cm^{-2}$ (black) that show less change in EQE than that of the reference device (magenta).

When assessing the contribution of radiation (particularly) to the devices via analysis of the EQE the orientation of the irradiation with respect to the illumination under operation should be considered. This is shown in figure 4(c) with respect to the EQE in figure 4(d). To enable site specific irradiation, proton irradiation was performed at the 'backside' of the device (right in figure 4(c)) through the ETL layers at which the gold electrodes are deposited allowing easy access to the absorber. Illumination is typically provided to the 'frontside' via the transparent glass substrate (left—figure 4(c)) which would inhibit proton exposure except for very high impractical energies. As such, although high energy (short wavelength) probes the top HTL region, the low energy (longer wavelength) light is absorbed deeper into the cell thorough the absorber into the back ETL region which is where most of the most prohibitive NIEL processes or defect generation typically occur due to low energy proton exposure (see figure 1(a)).

However, upon careful examination of the changes in EQE, it became evident that the front side of the device (HTL) is more significantly affected after transit and/or irradiation than the rest of the device. This indicates deterioration occurs at the hole transport layer (HTL), and that this loss is the primary reason for loss of performance of *all of the solar cells* under inspection. This further supports the conclusion that environmental rather than radiation induced degradation is the primary loss mechanisms in the devices assessed in this study, and that device instability here is dominated specifically by losses in the HTL; which is

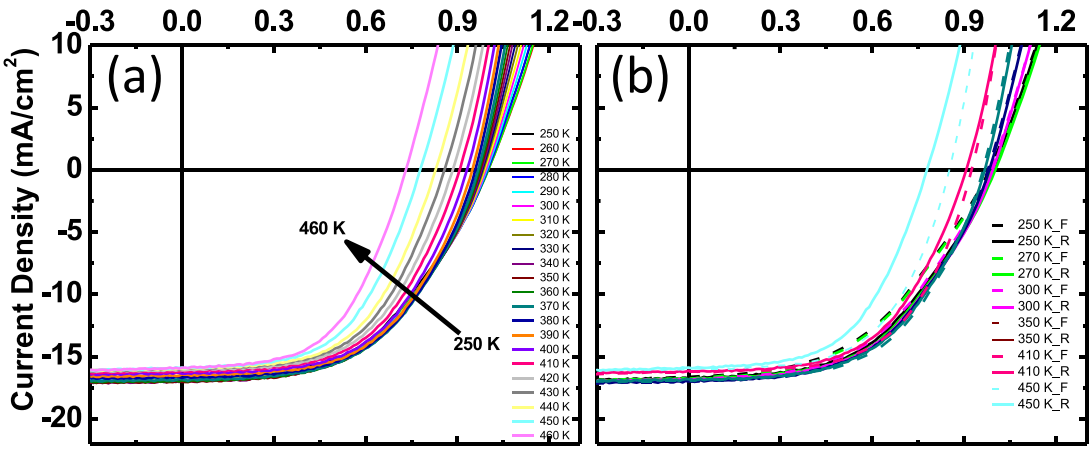


**Figure 5.** (a) Temperature dependent *J–V* for a pristine device. (b) Comparison of the forward and reverse hysteresis sweep for these devices at selected temperatures. Hysteresis increases at increasing temperature exposure.

likely due to environmental conditions such as high temperature exposure and humidity due to their transfer to and from North Texas (UNT) in the summer.

To further assess this hypothesis, and the role of temperature cycling on the devices, temperature dependent *J–V* measurements were performed on a pristine solar cell as shown in figure 5(a). The measurements were initiated at 250 K and increased in increments of 10 K until the device lost its PV behavior. Remarkably, despite some loss of voltage the solar cells continued to operate up to a temperature of ∼460 K.

The $J_{sc}$ measured was ∼17 mA cm$^{-2}$ throughout the temperature range studied while, the $V_{oc}$ is affected much more with increasing thermal load: decreasing gradually up to ∼380 K and then more sharply declines at higher temperatures. Similar results were seen in a previous study [6]. Such loss of voltage typically reflects increased non-radiative recombination and elevated dark currents leading to deterioration and loss of rectification, therefore performance in solar cells. In perovskite solar cells such losses have been attributed to factors such as the decomposition of the metal halide, which, while less prohibitive to the operation of these systems, does reduce the effective voltage [6], or a structural phase transition [45, 46]. Here, the EQE before and after thermal cycling indicate very little change in the band gap (supplementary information SI-3) suggesting some halide segregation rather than a structural phase transition.

However, without a complete structural analysis, a soft phase transition cannot be completely ruled out at the probed temperatures since this has also been shown to occur in these triple halide systems where decomposition affects structural stability in such systems [45]. Here, however, the losses in voltage and the comparative analysis of the devices under external perturbation indicate the losses observed here are more likely due to deterioration of the interfacial properties in the device, leading to pinning of the fermi-levels and increased recombination losses at the heterointerfaces [39]. This is supported by the hysteretic behavior in figure 5(b) that is evident at $T > 380$ K [47]. The presence of hysteresis clearly demonstrates a reduction in charge extraction and the loss of interfacial quality at elevated temperatures. Such effects have been reported for $NiO_x$/perovskite interfaces at elevated temperatures [48] and related to the formation of a non-perovskite interlayer at this interface which is resistive to hole collection [49].

## 3. Conclusion

In summary, this study supports the resilience of perovskite solar cells against radiation exposure, assessing the radiation response across the top and bottom device interface within the device stack via targeted proton irradiation. Though the tolerance of the devices to radiation is demonstrated, the sensitivity, particularly of the $NiO_x$/perovskite interface within these architectures, to environmental factors (such as temperature and humidity) during transportation indicate the critical need for a comprehensive assessment of the various device structures for space applications. Such assessment is crucial for ensuring the suitability of these systems for both the space environments and launch conditions, suggesting the potential need for device encapsulations.

## Data availability statement

The data that support the findings of this study are available upon reasonable request from the authors.

## Acknowledgments

The authors at OU acknowledge support from NASA EPSCoR Grant No.: 80NSSC23M0073, and the Center for Quantum Research and Technology (CQRT) at the University of Oklahoma. The authors at UNT acknowledge support from NSF Grant No. ECCS-2210722.

## ORCID iDs

Vincent R Whiteside https://orcid.org/0000-0001-7846-3150
Mritunjaya Parashar https://orcid.org/0000-0003-0943-3091
Ian R Sellers https://orcid.org/0000-0003-2782-0044

## References

[1] Wu T *et al* 2021 The main progress of perovskite solar cells in 2020–2021 *Nano-Micro Lett.* **13** 1–18
[2] Wu X *et al* 2020 Stable triple cation perovskite precursor for highly efficient perovskite solar cells enabled by interaction with 18C6 stabilizer *Adv. Funct. Mater.* **30** 1908613
[3] Durant B K, Afshari H, Singh S, Rout B, Eperon G E and Sellers I R 2021 Tolerance of perovskite solar cells to targeted proton irradiation and electronic ionization induced healing *ACS Energy Lett.* **6** 2362–8
[4] Christians J A, Schulz P, Tinkham J S, Schloemer T H, Harvey S P, Tremolet de Villers B J, Sellinger A, Berry J J and Luther J M 2018 Tailored interfaces of unencapsulated perovskite solar cells for $>$ 1,000 hour operational stability *Nat. Energy* **3** 68–74
[5] Wu M *et al* 2020 Stability issue of perovskite solar cells under real-world operating conditions *Energy Technol.* **8** 1900744
[6] Afshari H, Sourabh S, Chacon S A, Whiteside V R, Penner R C, Rout B, Kirmani A R, Luther J M, Eperon G E and Sellers I R 2023 FACsPb triple halide perovskite solar cells with thermal operation over 200° C *ACS Energy Lett.* **8** 2408–13
[7] Miyazawa Y, Ikegami M, Chen H-W, Ohshima T, Imaizumi M, Hirose K and Miyasaka T 2018 Tolerance of perovskite solar cell to high-energy particle irradiations in space environment *IScience* **2** 148–55
[8] Klein-Kedem N, Cahen D and Hodes G 2016 Effects of light and electron beam irradiation on halide perovskites and their solar cells *Acc. Chem. Res.* **49** 347–54
[9] Duan L *et al* 2023 Stability challenges for the commercialization of perovskite–silicon tandem solar cells *Nat. Rev. Mater.* **8** 261–81
[10] Fu F, Li J, Yang T C-J, Liang H, Faes A, Jeangros Q, Ballif C and Hou Y 2022 Monolithic perovskite-silicon tandem solar cells: from the lab to fab? *Adv. Mater.* **34** 2106540
[11] Tu Y, Wu J, Xu G, Yang X, Cai R, Gong Q, Zhu R and Huang W 2021 Perovskite solar cells for space applications: progress and challenges *Adv. Mater.* **33** 2006545
[12] Afshari H, Chacon S A, Sourabh S, Byers T A, Whiteside V R, Crawford R, Rout B, Eperon G E and Sellers I R 2023 Radiation tolerance and self-healing in triple halide perovskite solar cells *APL Energy* **1** 026105
[13] Alcaraz J *et al* 2000 Protons in near earth orbit *Phys. Lett.* B **472** 215–26
[14] Inguimbert C and Messenger S 2012 Equivalent displacement damage dose for on-orbit space applications *IEEE Trans. Nucl. Sci.* **59** 3117–25
[15] Yao Y, Cheng C, Zhang C, Hu H, Wang K and De Wolf S 2022 Organic hole-transport layers for efficient, stable, and scalable inverted perovskite solar cells *Adv. Mater.* **34** 2203794
[16] Mahmood K, Sarwar S and Mehran M T 2017 Current status of electron transport layers in perovskite solar cells: materials and properties *RSC Adv.* **7** 17044–62
[17] Jiang Q, Zhang X and You J 2018 $SnO_2$: a wonderful electron transport layer for perovskite solar cells *Small* **14** 1801154
[18] Zhu H, Zhang T-H, Wei Q-Y, Yu S-J, Gao H, Guo P-C, Li J-K and Wang Y-X 2022 Preparation of $TiO_2$ electron transport layer by magnetron sputtering and its effect on the properties of perovskite solar cells *Energy Rep.* **8** 3166–75
[19] Xie F, Chen -C-C, Wu Y, Li X, Cai M, Liu X, Yang X and Han L 2017 Vertical recrystallization for highly efficient and stable formamidinium-based inverted-structure perovskite solar cells *Energy Environ. Sci.* **10** 1942–9
[20] Cai X, Hu T, Hou H, Zhu P, Liu R, Peng J, Luo W and Yu H 2023 A review for nickel oxide hole transport layer and its application in halide perovskite solar cells *Mater. Today Sustain.* **23** 100438
[21] Paulescu M *et al* 2017 Experimental study of proton irradiation effect on silicon solar cells *AIP Conf. Proc.* **1796** 040010
[22] Dabbabi S, Ben Nasr T and Turki Kamoun N 2019 CIGS solar cells for space applications: numerical simulation of the effect of traps created by high-energy electron and proton irradiation on the performance of solar cells *JOM* **71** 602–7
[23] Warner J H, Walters R J, Messenger S R, Summers G P, Khanna S M, Estan D, Erhardt L S and Houdayer A 2004 High-energy proton irradiation effects in GaAs devices *IEEE Trans. Nucl. Sci.* **51** 2887–95
[24] Goodman S, Auret F D, Ridgway M and Myburg G 1999 Proton irradiation of n-type GaAs *Nucl. Instrum. Methods Phys. Res.* **148** 446–9
[25] Hirose Y, Warasawa M, Tsunoda I, Takakura K and Sugiyama M 2012 Effects of proton irradiation on optical and electrical properties of Cu (In, Ga) $Se_2$ solar cells *Jpn. J. Appl. Phys.* **51** 111802
[26] Chacon S A, Khanal M N, Durant B K, Afshari H, Byers T A, Parashar M, Rout B, Whiteside V R, Poplavskyy D and Sellers I R 2023 Probing the interfacial properties of ACIGS solar cells with targeted proton irradiation *Solar RRL* **8** 2300756
[27] Lang F *et al* 2021 Proton-radiation tolerant all-perovskite multijunction solar cells *Adv. Energy Mater.* **11** 2102246
[28] Lang F *et al* 2016 Radiation hardness and self-healing of perovskite solar cells *Adv. Mater.* **28** 8726–31

[29] Brus V V, Lang F, Bundesmann J, Seidel S, Denker A, Rech B, Landi G, Neitzert H C, Rappich J and Nickel N H 2017 Defect dynamics in proton irradiated $CH_3NH_3PbI_3$ perovskite solar cells *Adv. Electron. Mater.* **3** 1600438
[30] Barbé J, Hughes D, Wei Z, Pockett A, Lee H K H, Heasman K C, Carnie M J, Watson T M and Tsoi W C 2019 Radiation hardness of perovskite solar cells based on aluminum-doped zinc oxide electrode under proton irradiation *Solar RRL* **3** 1900219
[31] Kirmani A R *et al* 2022 Countdown to perovskite space launch: guidelines to performing relevant radiation-hardness experiments *Joule* **6** 1015–31
[32] Parkhomenko H P, Mostovyi A I, Akhtanova G, Solovan M M, Kaikanov M, Schopp N and Brus V V 2023 Self-healing of proton-irradiated organic photodiodes and photovoltaics *Adv. Energy Mater.* **13** 2301696
[33] Yu Y, Zhang F and Yu H 2020 Self-healing perovskite solar cells *Sol. Energy* **209** 408–14
[34] Stoller R E, Toloczko M B, Was G S, Certain A G, Dwaraknath S and Garner F A 2013 On the use of SRIM for computing radiation damage exposure *Nucl. Instrum. Methods Phys. Res.* **310** 75–80
[35] Kirmani A R *et al* 2023 Metal oxide barrier layers for terrestrial and space perovskite photovoltaics *Nat. Energy* **8** 191–202
[36] Young J M, Byers T A, Lang E J, Singh S, Glass G A, Hattar K and Rout B 2021 Synthesis of magnesiowüstite nanocrystallites embedded in an amorphous silicate matrix via low energy multiple ion implantations *Planet. Space Sci.* **206** 105319
[37] Zhao C, Chen B, Qiao X, Luan L, Lu K and Hu B 2015 Revealing underlying processes involved in light soaking effects and hysteresis phenomena in perovskite solar cells *Adv. Energy Mater.* **5** 1500279
[38] Brown C, Eperon G, Whiteside V and Sellers I 2018 Potential of high-stability perovskite solar cells for low-intensity–low-temperature (LILT) outer planetary space missions *ACS Appl. Energy Mater.* **2** 814–21
[39] Afshari H, Durant B K, Kirmani A R, Chacon S A, Mahoney J, Whiteside V R, Scheidt R A, Beard M C, Luther J M and Sellers I R 2022 Temperature-dependent carrier extraction and the effects of excitons on emission and photovoltaic performance in $Cs_{0.05}FA_{0.79}MA_{0.16}Pb(I_{0.83}Br_{0.17})_3$ solar cells *ACS Appl. Mater. Interfaces* **14** 44358–66
[40] Cheng Y, Meleco A J, Roeth A J, Whiteside V R, Debnath M C, Mishima T D, Santos M B, Hatch S, Liu H and Sellers I R 2017 An investigation of the role of radiative and nonradiative recombination processes in $InAs/GaAs_{1-x}Sb_x$ quantum dot solar cells *IEEE J. Photovolt.* **8** 487–92
[41] Ompong D and Singh J 2018 High open-circuit voltage in perovskite solar cells: the role of hole transport layer *Org. Electron.* **63** 104–8
[42] Aeronautics, A.I.o. and Astronautics 2019 *Qualification and Quality Requirements for Electrical Components on Space Solar Panels–Amendment 1 (AIAA S-112A-2013/A1-2019)* (American Institute of Aeronautics and Astronautics, Inc.)
[43] VanSant K T *et al* 2023 Combined stress testing of perovskite solar cells for stable operation in space *ACS Appl. Energy Mater.* **6** 10319–26
[44] Kirmani A R *et al* 2024 Unraveling radiation damage and healing mechanisms in halide perovskites using energy-tuned dual irradiation dosing *Nat. Commun.* **15** 696
[45] Schelhas L T *et al* 2019 Insights into operational stability and processing of halide perovskite active layers *Energy Environ. Sci.* **12** 1341–8
[46] Mundt L E *et al* 2021 Mixing matters: nanoscale heterogeneity and stability in metal halide perovskite solar cells *ACS Energy Lett.* **7** 471–80
[47] Liu P, Wang W, Liu S, Yang H and Shao Z 2019 Fundamental understanding of photocurrent hysteresis in perovskite solar cells *Adv. Energy Mater.* **9** 1803017
[48] Moot T *et al* 2021 Temperature coefficients of perovskite photovoltaics for energy yield calculations *ACS Energy Lett.* **6** 2038–47
[49] Kavadiya S, Onno A, Boyd C C, Wang X, Cetta A, McGehee M D and Holman Z C 2021 Investigation of the selectivity of carrier transport layers in wide-bandgap perovskite solar cells *Solar RRL* **5** 2100107